

Meta-GGAs vs. Hybrid Functionals for Point Defects: The Best of Both Worlds Applied to Layered MnO_2 , NiO_2 and KCoO_2

Raj K. Sah

Department of Physics, Temple University, Philadelphia, PA 19122

Michael J. Zdilla and Eric Borguet

Department of Chemistry, Temple University, Philadelphia, PA 19122

John P. Perdew

*Department of Physics and Engineering Physics,
Tulane University, New Orleans, LA 70118*

Defects in a material can significantly tune properties and enhance utility. Hybrid functionals like HSE06 are often used to describe solids with such defects. However, geometry optimization (including accounting for effects such as Jahn-Teller distortion) using hybrid functionals is challenging for the large supercells needed for defect study. The proposed $r^2\text{SCAN}+r\text{VV10}+U+U_d$ method, which is computationally much cheaper and faster than hybrid functionals, can successfully describe defects in materials with the proper choice of U (for the d orbitals of the host atom) and U_d (for those of the defect atom), as shown here for small polaron defects in layered transition-metal oxides. We use a literature value of U or U_d appropriate to a given transition-metal ion and its oxidation state. The layered materials birnessite ($\text{K}_n\text{MnO}_2, n = 0.03$) and $\text{K}_n\text{NiO}_2, n = 0.03$, with one K atom intercalated between layers in a supercell, are found to have one localized occupied e_g polaronic state on the transition metal ion reduced by the insertion of the K atom, when the geometry is calculated as above using published U values. The expected Jahn-Teller distortion is not observed when $U=U_d=0$. Layered cobalt oxide with additional potassium ions intercalated ($\text{K}_n\text{CoO}_2, n = 1.03$) is different, due to a dramatic difference in electronic configuration of the defected Co(II) ion: A single extra K atom in the supercell leads to four localized electrons in the band gap, using standard U values, and even for $U=U_d=0$.

I. INTRODUCTION

This work is part of a larger project on the computational identification of alkali-atom-intercalated layered materials as promising catalysts for the oxygen evolution reaction (OER) of water splitting for clean hydrogen production. Earlier work [1, 2] showed the importance of small-polaron defects formed by transfer of an electron from an intercalated alkali atom to a neighboring manganese ion. Calculation of the polaron often requires a nonlocal density functional for the exchange-correlation energy, and geometry optimization in a large supercell. We found that hybrid functionals as used in Ref.

[1] are too expensive for a broad materials search. In this article, we show that an alternative $r^2\text{SCAN}+r\text{VV10}+U+U_d$ approach can achieve comparable accuracy at much lower cost, and may be useful for other point defects in a range of materials. We also found that, while one intercalated K atom creates one localized electron in the energy gap of layered MnO_2 and NiO_2 , it can create four in layered KCoO_2 . We further found that, while $r^2\text{SCAN}$ needs a $+U$ correction to create a polaron in MnO_2 and NiO_2 , it does not need one in KCoO_2 . Our broader computational and experimental materials search is now underway.

Various types of defects exist in solids, and

defects in solids can influence numerous important properties like electrical conductivity, reactivity, and magnetic or optical properties. For example, the Oxygen Evolution Reaction (OER) is frequently favored by defects like polarons in transition metal oxide (TMO)-based catalysts [1, 2]. Leveraging defects as a tool allows fine tuning of the electronic properties of materials, making the understanding of defects in materials a pivotal area of research.

The computational design and study of such materials using first-principles density functional theory (DFT) [3, 4] offer valuable early insights. However, the approach presents challenges, as density functional approximations (DFAs) introduce self-interaction error (SIE). Popular DFAs such as LDA/GGA/meta-GGA tend to underestimate the Perdew-Parr-Levy-Baldurzi (PPLB) [5] straight line condition, leading to inaccuracies in describing charge transfer that are reduced but not eliminated in that sequence of functionals. Given that defect studies require proper charge transfer, DFAs often fall short in accurately portraying defects in a system.

Hybrid functionals, which combine a fraction of exact exchange, such as HSE06 [6] which utilizes 25% exact exchange and 75% PBE exchange in the short range along with full PBE exchange in the long range, experience less SIE and often provide a more accurate description of the electronic structure of materials. Hybrid functionals have been successfully employed in studying defects in solids. For instance, Peng et al. [1] effectively investigated polaron-like defects in birnessite (Fig. 1, $K_nMnO_2, n < 1$). Nevertheless, the inclusion of exact exchange in hybrid functionals renders them computationally expensive. The structural relaxation using hybrid functionals becomes particularly costly for a reasonably sized supercell with localized defects, with computational expenses rapidly escalating as the supercell size increases toward better simulation of defects. Consequently, the structural optimization of large supercells becomes impractical. An-

other challenge associated with hybrid functionals is that a material-independent exact exchange mixing parameter is not determined through any exact condition, nor is the range-separation parameter in range-separated hybrids [7]. Peng et al. determined a mixing parameter of 0.22 to study defects in birnessite using HSE06 [1], deviating from the original value of 0.25. Additionally, determining a mixing parameter for semiconductors that may not be suitable to metals or insulators [8] adds to the challenge of finding an appropriate parameter for the system under study when employing hybrid functionals.

r²SCAN [9] is a recently developed meta-generalized gradient approximation that reinstates exact constraint adherence to rSCAN [10], preserving the numerical efficiency of rSCAN while simultaneously restoring the transferable accuracy of SCAN [11]. Several studies have demonstrated that SCAN predicts geometries and other properties as well as or even better than hybrid functionals. Sun et al. [7] showed that SCAN accurately predicts geometries and energies of diversely bonded materials and molecules, matching or surpassing the accuracy of computationally expensive hybrid functionals. Another study by Sąnwick and Cocchi [12] on cesium-based photocathode materials Cs_3Sb and Cs_2Te reported excellent performance of SCAN and HSE06 for both structural and electronic properties. A recent paper on the arXiv [13] reports that, while SCAN may not reliably describe the properties of deep defects and small polarons in several semiconductors and insulators, it yields remarkably good agreement with experimental structural parameters for materials like ZnO , GaN , Ga_2O_3 and NaF . Additionally, a study by Varadwaj and Miyake [14] on the geometrical, electronic, and optical properties of vanadium dioxide found that SCAN and SCAN-rVV10 can adequately predict the most important geometrical and optoelectronic properties of VO_2 . Numerous related studies further support the idea that SCAN successfully describes the structure and other properties of materials. Given that r²SCAN closely

agrees with SCAN in accuracy, we expect that r^2 SCAN would exhibit similar accuracy in the aforementioned studies.

By construction, r^2 SCAN can exhibit very small or negligible SIE (as reflected by its smaller Hubbard U correction) and performs at the level of hybrid functionals but demands less computational resource and time. In this study, we demonstrate that the r^2 SCAN + rVV10 + U + U_d functional can effectively describe the defects in materials at the level of the hybrid functional HSE06, or possibly even better. Here, U represents the Hubbard U correction of Anisimov and collaborators [15–17], applied to transition metal sites other than the defect site, while U_d is the correction applied to the defect site. Cococcioni and de Gironcoli [18] showed that the + U correction can be regarded as a many-electron self-interaction correction that, like the PPLB condition [5], penalizes non-integer electron number on a localized orbital to which it is applied.

Additionally, vdW denotes the long-range van der Waal’s correction. In our approach, we utilize rVV10 [19, 20] to account for this interaction, which importantly reduces inter-layer spacing. In many of our calculations, including HSE06 without vdW, we use the supercell volume and shape from r^2 SCAN + rVV10 + U + U_d , although we can as a check relax the internal coordinates with HSE06.

Transition metal ions that serve as sites for defect formation in solids, are in different formal oxidation states (OS) than otherwise-identical ions. For example, in a K-intercalated MnO_2 , the polaronic Mn site is in the +3 OS and the remaining Mn ions are in the +4 oxidation state [1, 2]. Ions in different OS have different numbers of d electrons. Ref. [21] reports that the ideal U correction decreases with increasing OS, which is attributed to a lower number of exchange interactions among fewer d electrons in a higher oxidation state. This behavior has been observed and reported [21] for vanadium ions, and suggests $U_d > U$.

However, this situation is not universal, as

we can see that U values for Mn for r^2 SCAN are 1.5 eV, 2.1 eV and 1.8 eV for Mn ions with average oxidation states +3.5, +2.5 and +2.33 respectively [22]. Here we see that Mn in the +2.5 average OS needs more U correction than Mn in the +2.33 average OS, which does not follow the trend observed for vanadium, although U for Mn in the +3.5 average OS supports the trend within the same elemental series. However it is obvious for the Mn oxide system that Mn ions in different oxidation states need different U corrections. Another example for Co is found in Ref. [21], which found $U=3.0$ eV as a correction to SCAN for the oxidation reaction $6CoO+O_2 \rightarrow 2Co_3O_4$ (in which the Co ions are in the +2 and +2.67 oxidation states), but also found that SCAN with this U wrongly predicted the meta-stable crystal O1-CoO2 (in which the Co oxidation state is +4) to be non-metallic, while SCAN with $U=0$ correctly predicted it to be a metal. Thus the U value can vary with the oxidation state of ions in the system. This indicates that if a system has transition metal ions in different OS, the proper way to describe such a system would be to apply different U corrections to the transition metal ions based on their OS. This could be because DFAs make different SIE for ions in different OS.

Here we present a study of defects in solids by the double U correction r^2 SCAN + rVV10 + U + U_d method, where U_d is the U correction applied to the defect site and U is the U correction applied to remaining sites as required for the system. Since U typically increases with decreasing OS, and defect sites are typically in a lower oxidation state, we expect $U_d \geq U$, although exceptions are possible.

One can use the r^2 SCAN + rVV10 + U + U_d geometry and the HSE06 hybrid functional orbital energies to leverage the best features of the hybrid functional (e.g., band gap). It appears that employing the full r^2 SCAN + rVV10 + U + U_d and/or HSE06 using r^2 SCAN + rVV10 + U + U_d geometry is a state-of-the-art method for efficient

study of defects in solids.

II. RESULTS AND DISCUSSION

We choose three layered pristine TMOs, MnO_2 , NiO_2 , and KCoO_2 as the starting point for our study. Transition metal and oxygen ions in these TMOs are arranged in layers of MO6 (where $M=\text{Ni, Mn, Co}$) octahedra, with 32 transition metal ions per supercell. Inserting an additional potassium ion into the supercell between the layers creates a polaronic defect, specifically a Jahn-Teller electron small polaron [1]. This defect has been studied in birnessite (MnO_2) using the HSE06 functional [1].

A. Layered MnO_2

First, we calculated the one-electron density of states (DOS) for both the pristine (i.e., non-intercalated) and a K-intercalated birnessite (Fig. 1) using the HSE06 functional with an exact exchange mixing parameter (α) of 0.22 to reproduce the work of Peng et al. [1]. The resulting DOS are shown in Fig. 2. Comparing Figs. 2A and 2B in the current work with Figs. 2B and 2C of Peng et al [1], we conclude that we have successfully reproduced the latter's DOS results. We found the band gap of pristine birnessite to be 3.4 eV. Upon intercalation of a potassium (K) ion, we observed similar effects on the DOS as observed by Peng et al. [1]. In Fig. 2B, a K-intercalated birnessite exhibits the appearance of Mn(III) d-states at higher energy, a polaronic peak at the conduction band (CB) edge, and a break in spin symmetry of the total DOS in the CB. These effects were previously seen and explained by Peng et al. [1]. The shifting of d-states in the Mn(III) d-states is attributed to increased coulomb repulsion in d orbitals of Mn(III). The spin symmetry of the total DOS in pristine MnO_2 arises from the antiferromagnetic order of the Mn(IV) ions, and is disrupted by the defect Mn(III) ion (while the other pristine materials are non-magnetic). The appearance of

the polaron peak is attributed to e_g^1 states in Mn(III) [1, 2].

We will see similar effects upon a K-intercalation in NiO_2 and KCoO_2 systems later, and these effects can be understood through similar reasoning. The d-state electronic configurations of Mn(IV) in pristine MnO_2 and Mn(III) in a single-K-intercalated MnO_2 are as shown in Fig. 5 A and B respectively.

Swathilakshmi et al. [22] recently determined the optimal U value for $r^2\text{SCAN}$ for Mn to be 1.8 eV. They utilized three oxidation reactions: $\text{MnO} \rightarrow \text{Mn}_2\text{O}_3$, $\text{MnO} \rightarrow \text{Mn}_3\text{O}_4$, and $\text{Mn}_2\text{O}_3 \rightarrow \text{MnO}_2$. The U values for these reactions are 2.1 eV, 1.8 eV and 1.5 eV respectively [22]. The average OS of Mn ions in these reactions are +2.5, +2.3, and +3.5 respectively [22]. U values for these reactions are small compared to those for the PBE GGA and do not differ significantly, suggesting that $r^2\text{SCAN}$ makes a small, comparable SIE but not an equal one for Mn(II), Mn(III) and Mn(IV) ions in manganese oxide systems. The reported optimal U value of 1.8 eV for the Mn ion is the average of U values for the above three oxidation reactions [22].

First, we performed $r^2\text{SCAN} + r\text{VV10} + U$ calculations for pristine birnessite with the optimal U of 1.8 eV and obtained the DOS as shown in Fig. 3A. $r^2\text{SCAN} + r\text{VV10} + U$ predicts a band gap of 2.30 eV for the pristine structure. The underestimation of the band gap compared to HSE06 by meta-GGA/GGA is a well-known general trend [23]. Next, we performed $r^2\text{SCAN} + r\text{VV10} + U + U_d$ calculations for a K-intercalated MnO_2 . As $r^2\text{SCAN}$ exhibits a small SIE, we initially set $U=U_d=0.0$ eV to see the performance of $r^2\text{SCAN}+r\text{VV10}$ without U correction. However, this method failed to resolve the Jahn-Teller defect, as depicted in Fig. 3B. The corresponding electron from the K atom is delocalized, which can be seen by the extra electrons between the CB minimum and the chemical potential or Fermi level at 0 eV. This can be clearly seen in the inset of

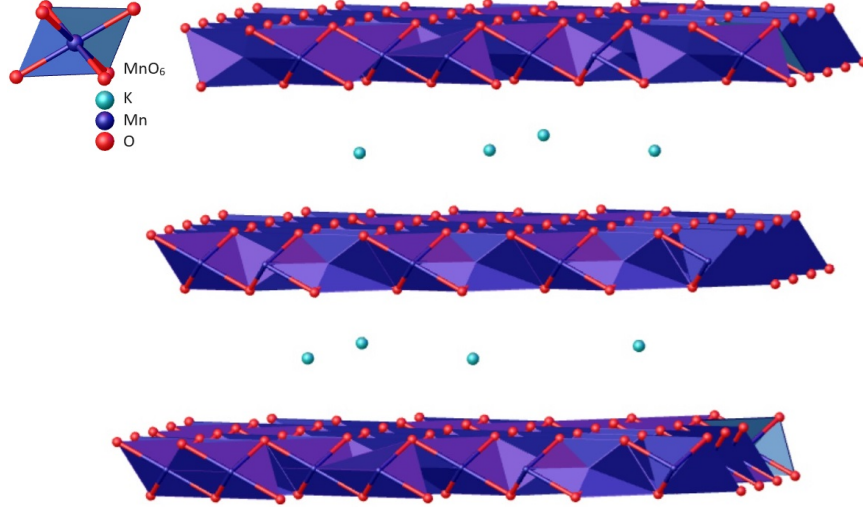


FIG. 1. General structure for layered potassium metal oxides K_nMnO_2 .

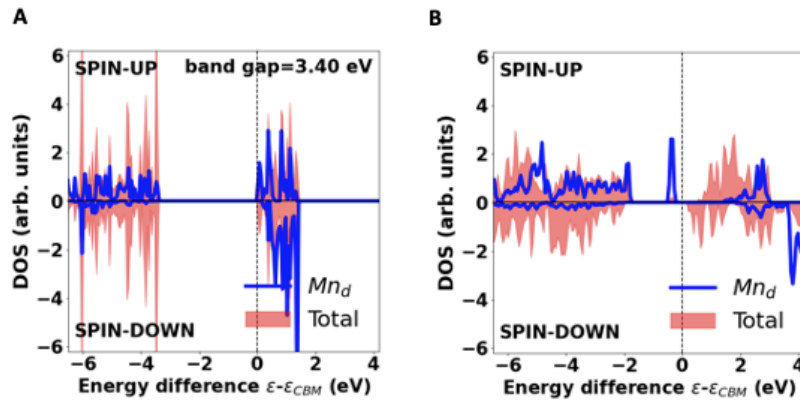


FIG. 2. HSE06 ($\alpha = 0.22$) spin-resolved density of states per atom in (A) pristine MnO_2 with Mn(IV) ions and (B) MnO_2 with a single intercalated K^+ ion and a defect Mn(III) cation in a supercell with 97 atoms. For comparison with Ref. [1], the interlayer spacing is set to 7.12 Å, and internal coordinates are relaxed in HSE06. In Figs. 1-9 (except in Figs. 5, and 8), the shaded area shows the total density of one-electron states, and the blue curve shows the transition-metal-d states projected onto the site where the small polaron forms or is expected to form. Also in Figs. 1-9 (except in Figs. 5, and 8), the peaks (if any) in the band gap below the conduction band minimum (CBM) are occupied, localized states of the defect ion. The energy zero is set to the energy of the lowest-energy unoccupied orbital. The total density has been scaled down to make it comparable in size to the projected Mn-d density of states.

Fig. 3B. For the description of a polaron in a single K-intercalated MnO_2 , DFA has to transfer charge from the inserted K atom to a Mn atom. The charge delocalization error of DFAs prohibits transferring a complete electron from the K atom to the Mn site. This indicates the need for +U correction,

which can remove the partial occupancy and localize the electron on the defect site. Subsequently, we tested the optimal U by setting $U=U_d=1.8$ eV and the obtained DOS is shown in Fig. 3C, revealing the appearance of a polaronic peak, and the appropriate distortion of Mn-O bonds at

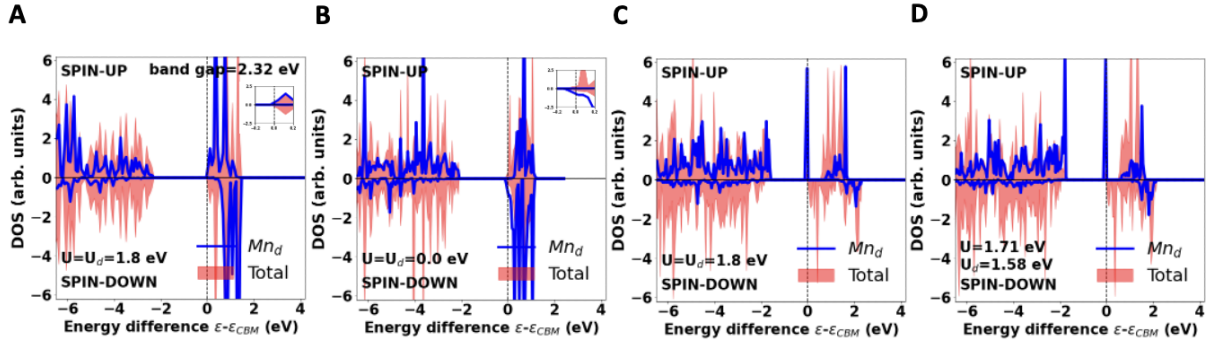


FIG. 3. r^2 SCAN+rVV10+U+ U_d spin-resolved density of states per atom in (A) pristine MnO_2 with $U=U_d=1.8$ eV and in a single K-intercalated MnO_2 with (B) $U=U_d=0.0$ eV, (C) $U=U_d=1.8$ eV, (D) $U=1.71$ eV and $U_d=1.58$ eV. The geometry has been optimized in r^2 SCAN+rVV10+U+ U_d , which makes the interlayer spacing 5.26 Å. The insets in Figs. A and B show the DOS near the 0 eV region. The inset of Fig. B shows that for $U=U_d=0$ the extra electron from the intercalated K goes to the bottom of the conduction band, making a semi-metal.

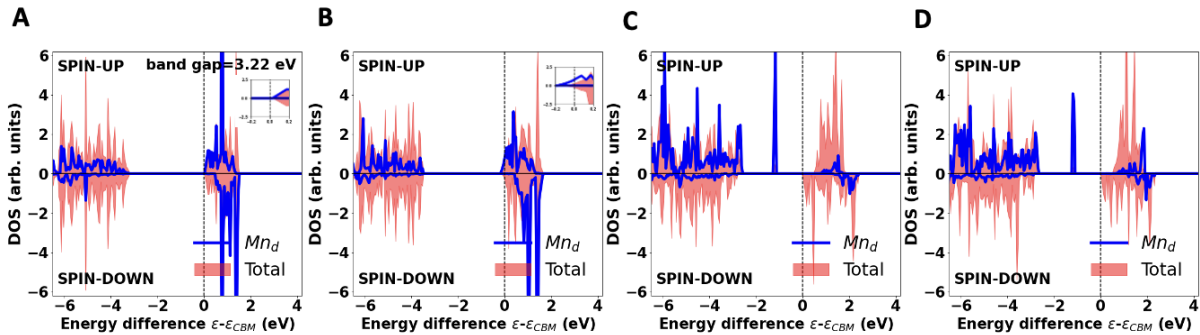


FIG. 4. HSE06($\alpha=0.25$)+D3 spin-resolved density of states per atom using r^2 SCAN+rVV10+U+ U_d geometry of Fig. 3 in (A) pristine MnO_2 with $U=U_d=1.8$ eV and in a single K-intercalated MnO_2 with (B) $U=U_d=0.0$ eV, (C) $U=U_d=1.8$ eV, (D) $U=1.71$ eV and $U_d=1.58$ eV. The insets in Figs. A and B show DOS near the 0 eV region. The inset in Fig. B shows that for $U=U_d=0$ the extra electron from the intercalated K goes to the bottom of the conduction band, making a semi-metal.

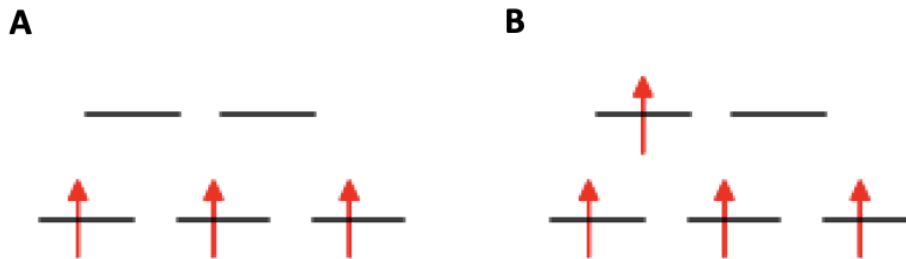


FIG. 5. d-orbital splitting (A) in Mn(IV) in pristine MnO_2 demonstrating filled t_{2g} states and empty e_g states and (B) in Mn(III) in a single K-intercalated MnO_2 .

the Jahn-Teller distorted manganese atom (see Fig. S2 B). The +U correction applies an energy penalty to the partially occupied orbital. As a result the polaron is localized and appears at the CB edge. We see shifting of Mn(III) d-states to higher energy, and spin symmetry breaking in the total DOS in the CB, consistent with the HSE06 results. As discussed in the work by Peng et al. [1] and Ding et al. [2], polaron formation can with the right distribution of intercalated potassium atoms create a potential step between layers that facilitates electron transfer between layers and enhances catalytic activity.

Motivated by studies indicating that U depends on OS, and that generally U decreases with an increase in OS, we determined U for the $r^2\text{SCAN}+r\text{VV10}+U$ functional for Mn(III) and Mn(IV) by comparing $r^2\text{SCAN}+r\text{VV10}+U$'s magnetic moment with the HSE06+D3 magnetic moment. For this we used pristine KMnO_2 and MnO_2 systems. First, we relaxed the structure using HSE06+D3 and used the structure to get the magnetic moment due to spin charge density within the Wigner-Seitz sphere around an Mn ion. We used the HSE06+D3 geometry for $r^2\text{SCAN}+r\text{VV10}+U$ and slowly increased U in small steps until we obtained the same magnetic moment as HSE06+D3. This method gave U values of 1.71 eV and 1.58 eV for Mn(III) and Mn(IV) ions, respectively. These values are close to the values in Ref. [22].

We then obtained the $r^2\text{SCAN}+r\text{VV10}+U+U_d$ DOS of a K intercalated MnO_2 with $U=1.71$ eV and $U_d=1.58$ eV which is as shown in Fig. 3C. $U=1.71$ eV and $U_d=1.58$ eV gave similar results to $U=U_d=1.8$ eV.

We also performed HSE06+D3 calculations on the $r^2\text{SCAN}+r\text{VV10}+U+U_d$ geometries, and the resulting DOS are plotted in Fig. 4. The D3 dispersion correction was used for the HSE06 functional with new D3 damping parameters $a1 = 0.383$, $a2 = 5.685$, and $s8 = 2.310$ generated for the HSE06 functional [24]. For HSE06+D3 calculations, we

used an exact exchange mixing parameter (α) of 0.25. This is because we found that the $r^2\text{SCAN}+r\text{VV10}+U$ geometry in much better agreement with the HSE06+D3 geometry for $\alpha=0.25$ than for 0.22. More details are in the Supplementary Material.

Fig. 4A shows the HSE06+D3 DOS of pristine MnO_2 obtained using the $r^2\text{SCAN}+r\text{VV10}+U+U_d$ ($U=U_d=1.8$ eV) geometry. HSE06+D3 increases the band gap of pristine MnO_2 , close to the HSE06 result (Fig. 2A). Fig. 4B shows the HSE06+D3 DOS of a K-intercalated MnO_2 obtained using the $r^2\text{SCAN}+r\text{VV10}+U+U_d$ ($U=U_d=0.0$ eV) geometry. Like the $r^2\text{SCAN}+r\text{VV10}+U+U_d$ ($U=U_d=0.0$ eV) method, HSE06+D3 also fails to localize the defect state due to the absence of the localized geometric distortion near a single Mn atom. Fig. 4C shows the HSE06+D3 DOS of a K-intercalated MnO_2 obtained using the $r^2\text{SCAN}+r\text{VV10}+U+U_d$ ($U=U_d=1.8$ eV) geometry. Here, the defect state appears as in the $r^2\text{SCAN}+r\text{VV10}+U+U_d$ ($U=U_d=1.8$ eV) method, but deep in the band gap. Fig. 4D shows the HSE06+D3 DOS of a K-intercalated MnO_2 obtained using the $r^2\text{SCAN}+r\text{VV10}+U+U_d$ ($U=1.71$ eV and $U_d=1.58$ eV) geometry. Here, also, the defect state appears as in the $r^2\text{SCAN}+r\text{VV10}+U+U_d$ ($U=U_d=1.8$ eV) method, but deep in the band gap.

We also calculated HSE06 and HSE06+D3 DOS using an exact exchange mixing parameter α of 0.22 as determined by Peng et al. [1] on $r^2\text{SCAN}+r\text{VV10}+U+U_d$ geometry with $U=U_d=1.8$ eV and obtained DOS as shown in Fig. S1 A and B, respectively. As expected, HSE06($\alpha=0.22$) and HSE06($\alpha=0.22$)+D3 DOS do not look different. Notably, the HSE06($\alpha=0.22$) DOS does not look different from the full HSE06($\alpha=0.25$)+D3 evaluated on the same geometry, which is shown in Fig. 4C.

R. Ding et al. [2] have proposed a position of the polaron close to the CB in layered MnO_2 with an alternation of polaron-rich and polaron-poor layers. This scenario matches better with $r^2\text{SCAN}+r\text{VV10}+U+U_d$ DOS,

where the polaron is close to the CB.

$r^2\text{SCAN}+r\text{VV10}+U+U_d$ with $U=U_d=1.8$ eV, and $U=1.71$ eV and $U_d=1.58$ eV give similar DOS. HSE06+D3 DOS are also similar for those geometries, with the polaron appearing deep in the gap.

It is challenging to conclude which method provides a better description of the defect. However, we can assert that all three methods- HSE06, $r^2\text{SCAN}+r\text{VV10}+U+U_d$ and HSE06+D3 using $r^2\text{SCAN}+r\text{VV10}+U+U_d$ geometry- have successfully described the polaronic defect in birnessite with the proper U and U_d for $r^2\text{SCAN}+r\text{VV10}+U+U_d$ calculations.

B. Layered NiO₂

Our next system under study was a layered NiO₂. This material has a hexagonal crystal structure with space group P6₃/mmc. The Materials Project website (<https://next-gen.materialsproject.org/>) reports that the material is synthesizable but not stable. Whether stable or not, this material is of interest for our study. Layered NiO₂ has a similar structure to birnessite, where Ni ions are in a +4 OS with completely occupied t_{2g} states, and empty e_g states [25].

We began the DOS calculation using the $r^2\text{SCAN}+r\text{VV10}+U+U_d$ functional for both pristine and K-intercalated NiO₂ systems. The $r^2\text{SCAN}$ U value for Ni ions was recently determined by Swathilakshmi et al. [22]. For the pristine NiO₂, $r^2\text{SCAN}+r\text{VV10}+U+U_d$ with $U=U_d=2.1$ eV, correctly predicts a non-magnetic ground state with a band gap of 1.62 eV, as shown in Fig. 6A. The d-states of Ni(IV) in pristine NiO₂ are split into t_{2g} and e_g states, with t_{2g} states completely occupied and e_g states empty, as shown in Fig. 8A. As in the birnessite case, we expect that adding an extra K atom between layers would transfer an electron from the inserted K atom to a Ni site, forming a defect. The defected Ni site would undergo Jahn-Teller distortion, localizing the electron in the e_g state, as shown in Fig. 8B.

For a K-intercalated NiO₂, we ini-

tially used $U=U_d=0.0$ eV to observe how $r^2\text{SCAN}+r\text{VV10}$ without U correction performs for this system, and we obtained the DOS as plotted in Fig. 6B. Again, this choice of U and U_d failed to describe the defect state, as can be seen from the inset in Fig. 6B. The extra electron goes to a delocalized state at the bottom of the conduction band, with fractional occupation on each Ni ion in the supercell, and no individual geometric distortion is observed at any nickel atom. We then used the available U value by setting $U=U_d=2.1$ eV and obtained the DOS, as plotted in Fig. 6C. This choice of U values forms a defect at one of the Ni sites, evidenced by the expected geometric distortion (see Fig. S3 B). The polaron is localized and appears in the gap just below the CB minimum. The formation of the polaron at the VB edge indicates that a K-intercalated NiO₂ could show OER catalytic activity similar to that of birnessite by lowering the overpotential. Most of the charge from the K atom is transferred to this defect site, which has a magnetic moment of $0.786 \mu_B$. However, we observe a Ni site in another layer picking up a small but nonzero magnetic moment of $0.137 \mu_B$, with the magnetic moment of all remaining Ni sites smaller than $0.03 \mu_B$. This suggests that we might need different values of U and U_d for $r^2\text{SCAN}+r\text{VV10}+U+U_d$ to accurately describe charge transfer to the defect site in a K-intercalated NiO₂ system.

The determination of $U=2.1$ eV for Ni for $r^2\text{SCAN}$ involves Ni in +2 and +3 states [22], with an average OS of +2.5. Since the precise U values for Ni(III) and Ni(IV) states are not available, we set $U_d=2.1$ eV for Ni(III) as the Ni (III) OS is close to +2.5 and searched for different U values for Ni(IV). We observed that increasing the U value beyond 2.3 eV transfers more and more charge to a Ni site in a layer different from that of the defect site. So, we lowered the U values ($U=1.0$ eV and 0.0 eV) and found that lowering the U values slightly improves the solution by lowering the magnetic moment of a Ni site in another layer to $0.06 \mu_B$ without significant

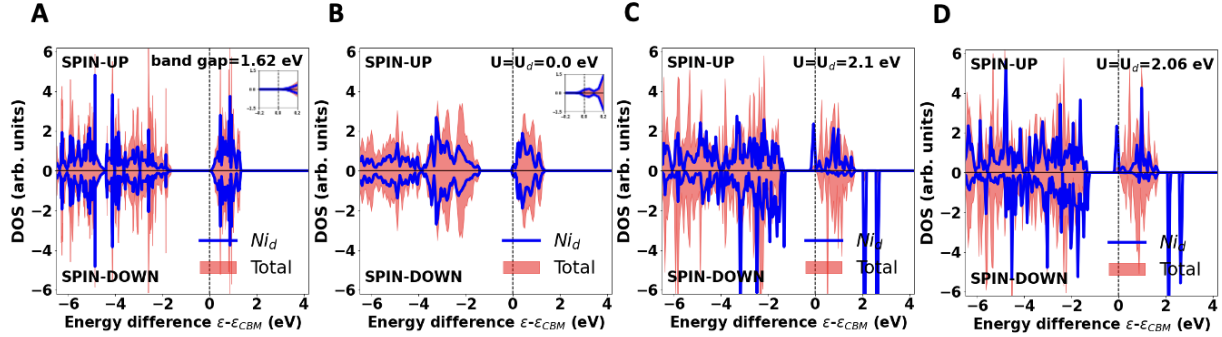


FIG. 6. $r^2\text{SCAN}+r\text{VV10}+U+U_d$ spin-resolved density of states per atom in (A) pristine NiO_2 with Ni(IV) ions with $U=U_d=2.1$ eV and in a single K-intercalated NiO_2 with (B) $U=U_d=0.0$ eV, (C) $U=U_d=2.1$ eV, (D) $U=U_d=2.06$ eV. The geometry was optimized in $r^2\text{SCAN}+r\text{VV10}+U+U_d$, which makes the interlayer spacing 5.42 Å. Here we can see one localized occupied state and several localized unoccupied states on the defect Ni(III) cation. The insets in Figs. A and B show the DOS near the 0 eV region. The inset in Fig. B shows that for $U=U_d=0$ the extra electron from the intercalated K goes to the bottom of the conduction band, making a semi-metal.

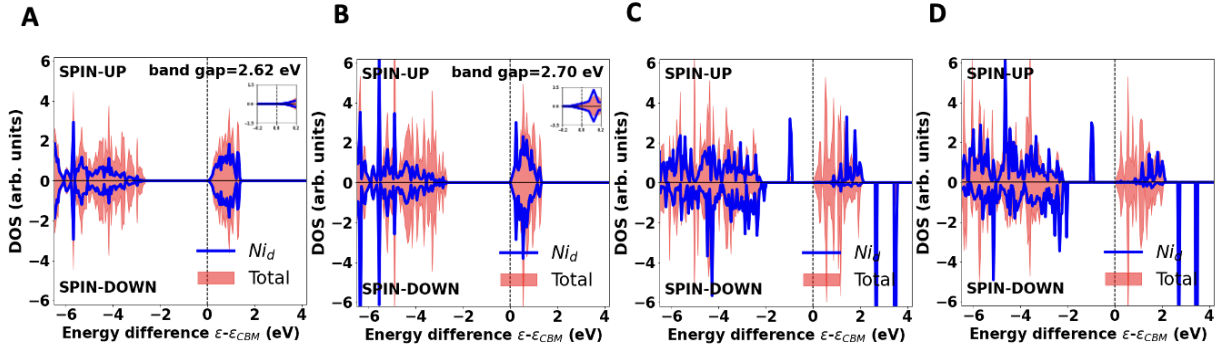


FIG. 7. HSE06+D3 spin-resolved density of states per atom using $r^2\text{SCAN}+r\text{VV10}+U+U_d$ geometry of Fig. 6 in (A) pristine NiO_2 with $U=U_d=2.1$ eV and a single K-intercalated NiO_2 with (B) $U=U_d=0.0$ eV and (C) $U=U_d=2.1$ eV, (D) $U=U_d=2.06$ eV. The insets in Figs. A and B show the DOS near the 0 eV region. The inset in Fig. B shows that for $U=U_d=0$ the extra electron from the intercalated K goes to the bottom of the conduction band, making a semi-metal.

change in magnetic moment of the defect site. The DOS plot for $U=0.0$ eV and $U_d=2.1$ eV do not look different from Fig. 6C. We also increased the U_d value, keeping U fixed at 2.1 eV, and observed an increase in the magnetic moment of the defect site, reaching $1 \mu_B$ for $U=3.8$ eV. These are the magnetic moments due to the spin density inside the Wigner-Seitz sphere. It is important to note that the magnetic moment of the defect site 1.0 does not guarantee the full transfer of an elec-

tron from the intercalated K atom to the defect site, as this is a magnetic moment inside the Wigner-Seitz sphere, which does not reflect the actual magnetic moment of the defect site. However, this analysis shows that one can adjust the U and U_d values for more charge transfer to the defect site where necessary.

We also determined the U value of 2.06 eV for the Ni(III) ion by equating the HSE06+D3 magnetic moment to the

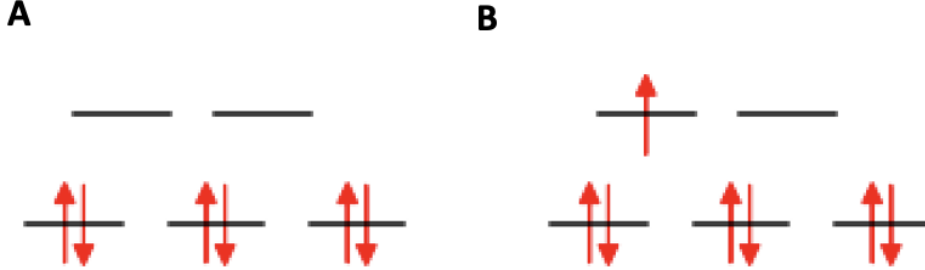


FIG. 8. d-orbital splitting (A) in Ni(IV) in pristine NiO₂ demonstrating filled t_{2g} states and empty e_g states and (B) in Ni(III) in a single K-intercalated NiO₂

r^2 SCAN+rVV10+U magnetic moment, as discussed in the Supplementary Material. As this value is not very different from 2.1 eV, we got a similar r^2 SCAN+rVV10+U+U_d result with $U=U_d=2.06$ eV compared to $U=U_d=2.1$ eV. Fig. 6D shows r^2 SCAN+rVV10+U+U_d DOS with $U=U_d=2.06$ eV.

Similar to birnessite, the d-states corresponding to Ni(III) in the VB are shifted to higher energy, as shown in Figs. 6C and 6D, and there is spin symmetry breaking on the total DOS in the CB. Here we do not claim $U=0.0$ eV to be the precise U value for Ni(IV) ions, but we suspect that U could be different than U_d for a K-intercalated NiO₂ system.

We also did HSE06+D3 calculations using the r^2 SCAN+rVV10+U+U_d geometry, and the results are shown in Fig. 7. We observe an increase in the band gap of pristine NiO₂, as shown in Fig. 7A. For a single K-intercalated NiO₂, due to the absence of a distorted nickel center, we do not observe polaron formation for $U=U_d=0.0$ eV, similar to r^2 SCAN+rVV10+U+U_d as shown in Fig. 7B; however, we observed an increase in the band gap. We also performed HSE06+D3 calculations for $U=U_d=2.1$ eV and for $U=U_d=2.06$ eV and obtained DOS as shown in Figs. 7C, and 7D, respectively. We observe an increase in the band gap and a shift of the polaron peak deep into the band gap region compared to the corresponding r^2 SCAN+rVV10+U+U_d DOS. We also observe other effects like shifting of Ni(III) d-states to higher energy and spin symmetry

breaking on the total DOS in the CB.

Both methods, full r^2 SCAN+rVV10+U+U_d and HSE06+D3 using the r^2 SCAN+rVV10+U+U_d geometry with proper U and U_d values, successfully describe defects in a single K-intercalated NiO₂. Among the methods employed to study defect in a K-intercalated NiO₂, full r^2 SCAN+rVV10+U+U_d is notably superfast.

C. Layered KCoO₂

We studied one final related layered material: KCoO₂, which has a hexagonal crystal structure with space group $P6_3/mmc$, similar to the above materials MnO₂ and NiO₂. The Materials Project website (<https://next-gen.materialsproject.org/>) shows a similar material, LiCoO₂, with space group $P6_3mc$, to be synthesizable but not stable. The electronic configuration of cobalt d-states is distinct from that of Mn and Ni, as illustrated in Fig. 1 in Ref. [2]. The optimal U value determined for Co ions for r^2 SCAN is 1.8 eV [22].

First, we calculated the DOS of KCoO₂ using the optimal U value of 1.8 eV, as shown in Fig. 9A. We observed symmetry in the spin resolved total DOS and Co d-states projected onto a Co site. This suggests that Co(III) ions in KCoO₂ have zero spin. The zero spin of Co(III) is also reported in the work of Chen et al. [26]. The d-state config-

uration of Co(III) is as shown in Fig. 11A.

The pristine CoO_2 has cobalt d states in a d^5 configuration, and KCoO_2 has cobalt in a d^6 configuration. A K-intercalated $\text{K}_{1.03}\text{CoO}_2$ would have a defect cobalt site in a d^7 configuration, with the remaining Co ions in a d^6 configuration. It is interesting to note that the Co(III) ion has no unpaired electron, but Co(II) has three unpaired electrons due to a low-spin to high-spin crossover [26–29]. So, unlike one electron in e_g , the state of defected Ni(III) and Mn(III), defected Co(II) has two electrons in the e_g states, with d-state configuration $t_{2g}^5 e_g^2$ (Figure 11 B, C) [27].

We performed $r^2\text{SCAN}+r\text{VV10}+U+U_d$ calculations to study the defects in a K-intercalated KCoO_2 . First, we tried $U=U_d=0.0$ eV to see how $r^2\text{SCAN}+r\text{VV10}$ performs without U correction, and obtained a DOS as shown in Fig. 9B. The blue plot, which is the projected density of states (PDOS) of d-states of the Co(II) ion, shows a significant change in the d-state of Co(II) compared to the d-state of Co(III) ion. Our calculation shows the magnetic moment of the Co(II) ion around 3, indicating three unpaired electrons in d-states. The presence of three unpaired electrons was previously seen in Refs. [26–29]. We observed Co(II) d-state splitting, as shown in Fig. 11B. This explains the appearance of Co(II) d-states just above the VB maximum in both channels, absence of Co(II) d-states in the CB in the up channel and presence in the down channel. There is a breaking of spin symmetry in the DOS, due to the appearance of a spin moment on the defected Co ion. The phenomena like shifting of d-states to higher energy and spin symmetry breaking in CB are similar to those observed and explained before in Peng et al.’s work [1] in the study of birnessite.

Then we used $U=U_d=1.8$ eV in $r^2\text{SCAN}+r\text{VV10}+U+U_d$ and obtained a DOS as shown in Fig. 9C. We do not see much difference between the $r^2\text{SCAN}+r\text{VV10}+U+U_d$ DOS for $U=U_d=0.0$ eV and $U=U_d=1.8$ eV. This indicates that the occupied Kohn-Sham orbitals are well localized and there is no fractional occupancy

in $r^2\text{SCAN}+r\text{VV10}+U+U_d$ calculations with $U=U_d=0.0$ eV. However, the larger U appears to bring peaks of the defected Co(II) d-states closer together in the band gap region just above the VB maximum.

As discussed in the Supplementary Material, we tried to determine the U value for the Co(II) ion by equating the HSE06+D3 magnetic moment to the $r^2\text{SCAN}+r\text{VV10}+U$ magnetic moment and obtained the U value for the Co(II) ion to be 0.91 eV. We used $U=U_d=0.91$ eV and obtained a DOS as shown in Fig. 9D, which looks similar to Figs. 9B and 9C.

We tried to compare a full HSE06+D3 DOS with $r^2\text{SCAN}+r\text{VV10}+U+U_d$ for pristine KCoO_2 and a K-intercalated KCoO_2 . We obtained the KCoO_2 supercell by inserting a K layer for each CoO_2 layer. Compared to the pristine CoO_2 supercell, which contains 96 ions, the KCoO_2 supercell has 32 extra K ions, and the K-intercalated KCoO_2 supercell has 33 extra K ions. Therefore, one would expect a different lattice parameter for KCoO_2 and a K-intercalated KCoO_2 , which requires the full relaxation of the supercell. We attempted to optimize the structure using the HSE06+D3 method, but it is very challenging for these systems in terms of time and resource. After a month, we chose not to proceed further. This challenge highlights one of the important reasons that motivated us to explore the $r^2\text{SCAN}+r\text{VV10}+U+U_d$ method, highlighting the significance of the $r^2\text{SCAN}$ meta-GGA for defect studies.

However, we calculated the HSE06+D3 DOS using $r^2\text{SCAN}+r\text{VV10}+U+U_d$ geometry. As shown in Fig. 10A, HSE06+D3 predicts KCoO_2 to be non-magnetic with an increased band gap of 4.17 eV. For a K-intercalated system with $r^2\text{SCAN}+r\text{VV10}+U+U_d$ geometry, the HSE06+D3 DOS is shown in Figs. 10 B, C, and D for $U=U_d=0.0$ eV, 1.8 eV, and 0.91 eV, respectively. Here we see that HSE06+D3 not only opens the gap between VB and CB, but it also brings the peaks of the defected Co(II) d-states closer together in the band gap region just above the VB maximum. We

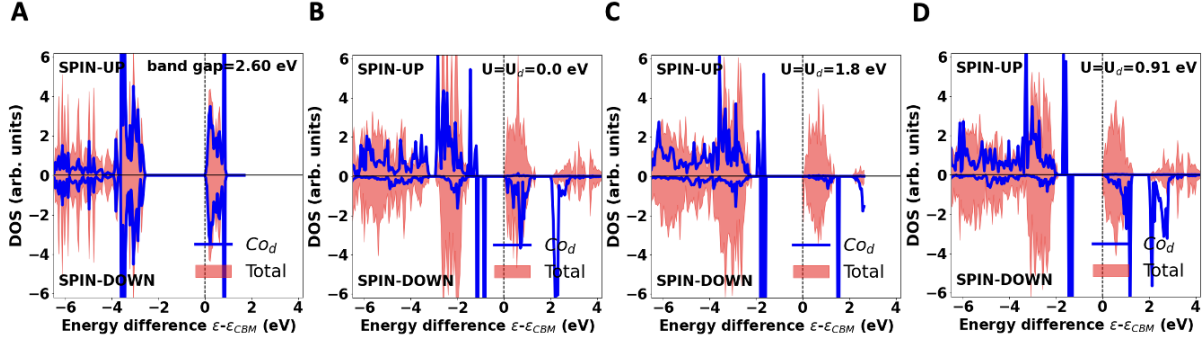


FIG. 9. $r^2\text{SCAN}+r\text{VV10}+U$ spin-resolved density of states per atom in (A) pristine KCoO_2 with Co(III) ions with $U=U_d=1.8$ eV, a single K-intercalated KCoO_2 with (B) $U=U_d=0.0$ eV, (C) $U=U_d=1.8$ eV, (D) $U=U_d=0.9$ eV. The more complicated pattern of in-gap states could reflect a Co(II) configuration different from a single unpaired electron in an e_g state. Here we see the appearance of several localized occupied states on the defect Co(II) cation. The geometry was optimized in $r^2\text{SCAN}+r\text{VV10}+U+U_d$, which makes the interlayer spacing 5.98 Å. Like the d-states of Ni(IV) , Co(III) has no electron in the e_g state and completely filled t_{2g} states. But, unlike the d-state of Ni(III) , which has only one electron in the e_g state and completely filled t_{2g} states, Co(II) has four electrons in e_g states, two in each channel, and partially filled t_{2g} states, as shown in Fig. 11B. The DOS peaks appearing in up and down channels in the gap region of a K-intercalated KCoO_2 are due to the e_g electrons in the up and down channels of Co(II) , respectively.

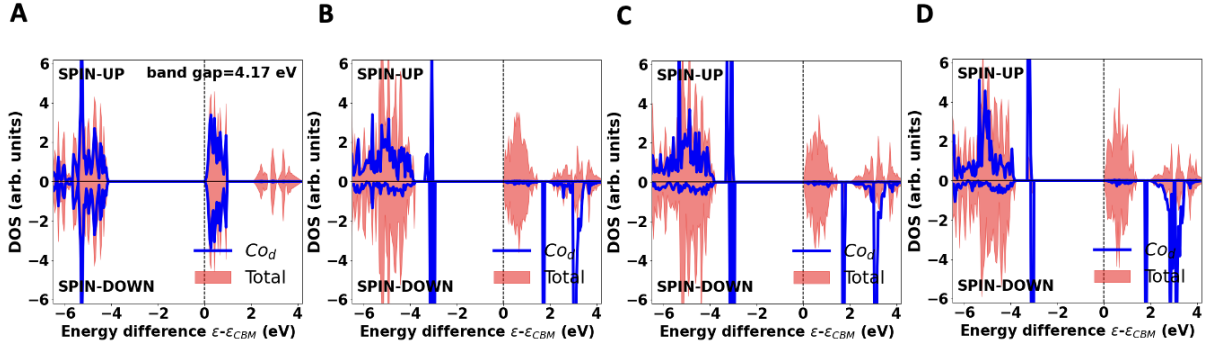


FIG. 10. $\text{HSE06}+\text{D3}$ spin-resolved density of states per atom using $r^2\text{SCAN}+r\text{VV10}+U+U_d$ geometry of Fig. 9 in (A) pristine KCoO_2 with $U=U_d=1.8$ eV, and in a single K-intercalated KCoO_2 with (B) $U=U_d=0.0$ eV, (C) $U=U_d=1.8$ eV, and (D) $U=U_d=0.9$ eV.

observed Co(II) d-states splitting as shown in Fig. 11C for the $\text{HSE06}+\text{D3}$ calculation using the $r^2\text{SCAN}+r\text{VV10}+U+U_d$ geometry with $U=U_d=1.8$ eV.

Fig. 11 shows our electronic configurations for Co(III) and Co(II) in octahedral or nearly octahedral coordination with oxygen. For Co(II) , we have seven d electrons. There are three t_{2g} orbitals of each spin, and two e_g

orbitals of each spin, and we can put no more than one electron into each spin orbital. Our output tells us the relative energy order of each occupied d state of each spin, that the net spin is nearly that of three spin-up electrons, and that the lowest-energy orbitals are spin-up while the highest-occupied orbital is spin-down, but not whether a given spin orbital is t_{2g} or e_g . So we begin by putting three

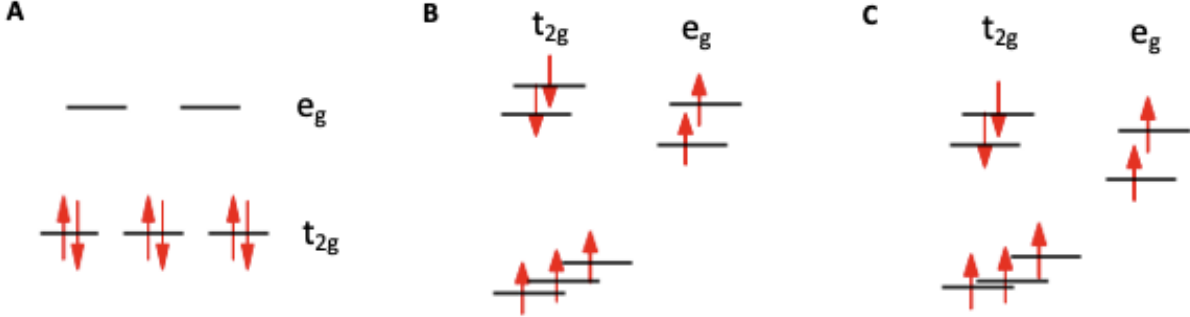


FIG. 11. Schematic diagram of energy of d-orbitals in (A) Co(III) in pristine KCoO_2 based on HSE06+D3 calculation using $r^2\text{SCAN} + r\text{VV10} + U + U_d$ geometry with $U = U_d = 1.8$ eV, (B) Co(II) in a single K-intercalated KCoO_2 based on orbital energy from $r^2\text{SCAN} + r\text{VV10} + U + U_d$ calculation with $U = U_d = 1.8$ eV and (C) Co(II) in a single K-intercalated KCoO_2 based on orbital energies from the HSE06+D3 calculation using the $r^2\text{SCAN} + r\text{VV10} + U + U_d$ geometry with $U = U_d = 1.8$ eV.

spin-up electrons into t_{2g} orbitals, to minimize the electronic repulsion. We assume that the e_g electrons prefer to be spin-up, to take advantage of an exchange interaction with the three up-spin t_{2g} orbitals, and that spin-up e_g levels will compete in energy with the spin-down t_{2g} levels. Then the configuration will be the one shown in Fig. 11 B and C, $(t_{2g} \uparrow)^3 (t_{2g} \downarrow)^2 (e_g \uparrow)^1 (e_g \downarrow)^1$. This result agrees with the $(t_{2g})^5 (e_g)^2$ configuration found for Co(II) in Li_2CoO_2 in Ref. [27]. This electronic configuration is also supported by the total charge density plots (see Fig. S5) of the four localized orbitals that appear in the band gap region of $\text{K}_{1.03}\text{CoO}_2$.

Regardless of coordination, Co(II) has been found to have a net spin nearly equal to that of three spin-up electrons in Refs. [26–29], but the distribution over t_{2g} and e_g of course depends upon coordination and other details of the nearby environment.

Fig. S4 B of the Supplementary Material shows the Jahn-Teller distorted tetrahedron around a defect Co(II) ion, with two of the Co(II)-O bonds about 10% longer than the remaining four. The angles are also distorted.

III. CONCLUSIONS

Defects in solids can be utilized to tune the electronic structure of materials, impacting applications in various fields. Defects

can be investigated using first-principles calculations with DFT. However, DFAs introduce SIE that could vary depending on the element, system, site, and oxidation state, hindering the performance of DFAs. Hybrid functionals mitigate SIE by mixing exact exchange, but at the expense of computational cost, successfully describing defects in many materials. The computational cost of hybrid functionals increases significantly for a SCF (self-consistent field) calculation compared to meta-GGAs like $r^2\text{SCAN}$. Defect studies require large supercells, making SCF calculations very expensive. Ionic relaxation calculations for defect studies involve many SCF cycles, making the process cumbersome for a hybrid functional to optimize the structure.

Here we demonstrate that the $r^2\text{SCAN} + r\text{VV10} + U + U_d$ method can successfully describe defects in materials with proper values of U and U_d . The method is much faster than hybrid functionals but equally accurate. Using the $r^2\text{SCAN} + r\text{VV10} + U + U_d$ geometry enables the completion of hybrid functional calculations in a reasonable time and with fewer resources. This approach makes hybrid functional calculations feasible for larger systems with transition-metal ions.

The $r^2\text{SCAN} + r\text{VV10} + U + U_d$ method proposed here is not only faster but also as accurate as the already established hybrid

functional method for defect studies. This method can expedite the study of defects in materials. The $r^2\text{SCAN}+r\text{VV10}+U+U_d$ method can also be employed in systems without defects where ions of the same species are in different OS.

We have studied the layered oxides MnO_2 , NiO_2 , and KCoO_2 , both in the pristine state and with one additional K atom intercalated between layers in a supercell. Inexpensive $r^2\text{SCAN}+r\text{VV10}+U+U_d$ equilibrium geometries have been used for electronic structure calculations with $r^2\text{SCAN}+r\text{VV10}+U+U_d$ and with the expensive HSE06 hybrid functional. For K-intercalated MnO_2 and NiO_2 , we find no localized e_g state on the defected transition metal ion for $U=U_d=0$, but we find one such state for standard positive U values. This state, in the gap between conduction and valence bands, accepts the electron donated by the intercalated K. (For $U=U_d=0$, the extra electron from the intercalated K goes into the bottom of the conduction band, making the intercalated material a semi-metal. The extra electron is then delocalized over the supercell, with fractional occupation on each transition-metal ion.)

For K-intercalated KCoO_2 , both for $U=U_d=0$ (standard semilocal $r^2\text{SCAN}$ without a nonlocal $+U$ self-interaction correction) and for standard positive U values, we seem to find two majority-spin and two minority-spin occupied localized e_g states in the gap between valence and conduction bands, and three empty localized minority-spin t_{2g} states in the gap above the conduction band. This surprising result is consistent with a dramatic change in the electronic configuration (Fig. 11) from the undefected Co(III) ions to the defected Co(II) ion, as reported previously in Ref. [26].

The $r^2\text{SCAN}+r\text{VV10}+U+U_d$ approach is successful, but it has limitations. It requires material-dependent parameters U , and those are typically available for only a few oxidation states of each transition metal. We have suggested a way to supplement the available values by choosing U to match the HSE06 magnetic moments, but that does not

work when a moment is zero. A possibly more satisfactory approach would be to do $r^2\text{SCAN}+r\text{VV10}+U$ calculations for isolated transition-metal ions with integer M and half-integer $M+1/2$ electron numbers. Since the $+U$ correction should be much less important for integer than for half-integer electron number, one can use $U(M+1/2)$ for both M and $M+1$. Then $U(M+1/2)$ could be found to satisfy the PPLB [5] condition $E(M+1/2) = [E(M+1)+E(M)]/2$, and $U(M')$ could be found for all M' by interpolation of $U(M'+1/2)$, yielding a set of oxidation-state-dependent values for each transition element. This possibility, which requires further thought and computation, is under consideration now in our group. Useful transfer of U from the free ion to the ion in a solid is not guaranteed, but the ratios of the U values for one element in different oxidation states might transfer better.

IV. COMPUTATIONAL DETAILS

First-principles calculations were performed with the projector-augmented wave method [30], implemented in the VASP code [31, 32]. A $4 \times 4 \times 1$ supercell was used to simulate defects in layered TMOs. For all supercell calculations, a $2 \times 2 \times 2$ Γ -centered Monkhorst-Pack k mesh [33] was used.

For $r^2\text{SCAN}+r\text{VV10}+U+U_d$ calculations, a 500 eV cutoff for the plane waves was used. In all $r^2\text{SCAN}+r\text{VV10}+U+U_d$ calculations, the cell volume was relaxed with the ISIF=3 setting until forces converged to less than $0.03 \text{ eV}/\text{\AA}$ and energy converged to less than 10^{-6} eV . To conduct $r^2\text{SCAN}+r\text{VV10}+U+U_d$ calculations, we employed the simplified rotationally invariant framework developed by Dudarev et al. [34].

For HSE (as for $r^2\text{SCAN}+r\text{VV10}+U+U_d$), corrections due to the periodic boundary condition and the supercell size have been added [1, 35]. For Fig. 2, we used an exact mixing parameter α of 0.22 in the hybrid functional HSE06 [1, 36], as determined from the Generalized Koopman's Condition

(GKC) method [37–40]. For all the remaining HSE06+D3 calculations, we used the standard exact exchange mixing parameter of 0.25. A plane-wave basis with an energy cutoff of 400 eV was employed.

V. ACKNOWLEDGMENTS

This work was supported by the U.S. Department of Energy, Office of Science Basic Energy Sciences under Award No.

DE-SC0023356.

VI. SUPPLEMENTARY MATERIAL

Determining a U parameter from the HSE06 magnetic moment. Effect of the D3 dispersion correction on lattice constants and density of states. Jahn-Teller symmetry breaking of the CoO6 tetrahedron in a single K-intercalated KCoO₂.

-
- [1] H. Peng, I. G. McKendry, R. Ding, A. C. Thenuwara, Q. Kang, S. L. Shumlas, D. R. Strongin, M. J. Zdilla, and J. P. Perdew, *PNAS* **114**, 9523 (2017).
- [2] R. Ding, P. Yasini, H. P. Peng, J. P. Perdew, E. Borguet, and M. J. Zdilla, *Adv. Energy Mater.* **11**, 2101636 (2021).
- [3] P. Hohenberg and W. Kohn, *Phys. Rev.* **136**, B864 (1964).
- [4] W. Kohn and L. J. Sham, *Phys. Rev.* **140**, A1133 (1965).
- [5] J. P. Perdew, R. G. Parr, M. Levy, and J. L. Balduz, Jr., *Phys. Rev. Lett.* **49**, 1691 (1982).
- [6] A. V. Krukau, O. A. Vydrov, A. F. Izmaylov, and G. E. Scuseria, *J Chem Phys* **125**, 224106 (2006).
- [7] J. Sun, R. C. Remsing, Y. Zhang, Z. Sun, A. Ruzsinszky, H. Peng, Z. Yang, A. Paul, U. Waghmare, X. Wu, M. L. Klein, and J. P. Perdew, *Nature Chemistry* **08**, 831 (2016).
- [8] T. M. Henderson, J. Paier, and G. E. Scuseria, *Phys. Status Solidi B* **248**, 767 (2011).
- [9] J. W. Furness, A. D. Kaplan, J. Ning, J. P. Perdew, and J. Sun, *J. Phys. Chem. Lett.* **11**, 8208 (2020).
- [10] A. P. Bartók and J. R. Yates, *J. Chem. Phys.* **150**, 161101 (2019).
- [11] J. W. Furness, A. D. Kaplan, J. Ning, and J. P. Perdew, *J. Phys. Chem. Lett.* **11**, 8208 (2020).
- [12] H.-D. Saýnick and C. Cocchi, *Electron. Struct.* **3**, 027001 (2021).
- [13] D. Wickramaratne and J. L. Lyons, *ArXiv:2311.03634v1*.
- [14] A. Varadwaj and T. Miyake, *ChemistrySelect* **7**, e202200171 (2022).
- [15] V. I. Anisimov, J. Zaanen, and O. K. Andersen, *Phys. Rev. B* **44**, 943 (1991).
- [16] V. I. Anisimov, I. V. Solovyev, M. A. Korotin, M. T. Czyzyk, and G. A. Sawatzky, *Phys. Rev. B* **48**, 16929 (1993).
- [17] I. V. Solovyev, P. H. Dederichs, and V. I. Anisimov, *Phys. Rev. B* **50**, 16861 (1994).
- [18] M. Cococcioni and S. de Gironcoli, *Phys. Rev. B* **71**, 035105 (2005).
- [19] O. A. Vydrov and T. V. Voorhis, *J. Chem. Phys.* **133**, 244103 (2010).
- [20] R. Sabatini, T. Gorni, and S. de Gironcoli, *Physical Review B* **87**, 041108 (2013).
- [21] O. Y. Long, G. S. Gautam, and E. A. Carter, *Physical Review Material* **4**, 045401 (2020).
- [22] S. Swathilakshmi, R. Devi, and G. S. Gautam, *J. Chem. Theory Comput.* **19**, 4202 (2023).
- [23] E. N. Brothers, A. F. Izmaylov, J. O. Normand, V. Barone, and G. E. Scuseria, *THE JOURNAL OF CHEMICAL PHYSICS* **129**, 011102 (2008).
- [24] J. Jonas and S. Grimme, *J. Phys. Chem. C* **118**, 7615 (2014).
- [25] J. M. P. Martirez and E. A. Carter, *J. Am. Chem. Soc.* **141**, 693 (2019).

- [26] J. Chen, X. Wu, and A. Selloni, *Phys. Rev. B* **83**, 245204 (2011).
- [27] G. Sun, F.-D. Yu, M. Lu, Q. Zhu, Y. Jiang, Y. Mao, J. A. McLeod, J. Maley, J. Wang, J. Zhou, and Z. Wang, *Nature Communications* **13**, 6464 (2022).
- [28] P. C. Bunting, M. Atanasov, E. Damgaard-Møller, M. Perfetti, I. Crassee, M. Orlita, J. Overgaard, J. V. Slageren, F. Neese, and J. R. Long, *Science* **362**, 1378 (2018).
- [29] W. J. Kim, M. A. Smeaton, C. Jia, B. H. Goodge, B. G. Cho, K. Lee, M. Osada, D. Jost, A. V. Ievlev, B. Moritz, L. F. Kourkoutis, T. P. Devereaux, and H. Y. Hwang, *Nature* **615**, 237 (2023).
- [30] P. E. Blöchl, *Phys. Rev. B* **50**, 17953 (1994).
- [31] G. Kresse and J. Hafner, *Phys. Rev. B Condens Matter* **49**, 14251–14269 (1994).
- [32] G. Kresse and D. Joubert, *Phys. Rev. B* **59**, 1758–1775 (1999).
- [33] H. Monkhorst and J. Pack, *Phys. Rev. B* **13**, 5188–5192 (1976).
- [34] S. L. Dudarev, G. A. Botton, S. Y. Savrasov, C. J. Humphreys, and A. P. Sutton, *Phys. Rev. B* **57**, 1505 (1998).
- [35] Y. Kumagai and F. Oba, *Phys. Rev. B* **89**, 195205 (2014).
- [36] A. Krukau, O. Vydrov, A. Izmaylov, and G. Scuseria, *J. Chem. Phys.* **125**, 224106 (2006).
- [37] S. Lany and A. Zunger, *Phys. Rev. B* **80**, 085202 (2009).
- [38] S. Lany, *Phys. Status Solidi B* **248**, 1052–1060 (2011).
- [39] H. Peng and S. Lany, *Phys. Rev. B* **85**, 201202 (2012).
- [40] H. Peng, P. Ndione, D. Ginley, A. Zakutayev, and S. Lany, *Phys. Rev. X* **5**, 021016 (2015).

Supplementary Material

Determination of Hubbard U from Magnetic Moment

To determine a Hubbard U for some of our calculations, we equated the HSE06+D3 magnetic moment (MM) of ions inside the Wigner-Seitz sphere with the r²SCAN+rVV10+U's MM. First, we relaxed the structure using the HSE06+D3 method and used this structure to calculate the HSE06+D3 MM. We then used the HSE06+D3 structure to do the r²SCAN+rVV10+U calculation, where we slowly varied the U value until r²SCAN+rVV10+U's MM becomes equal to the HSE06+D3's MM. We used smaller bilayer unit cells of transition metal oxides for U determination using this method. We used MnO₂, KMnO₂, KNiO₂, and CaCoO₂ to get U values for Mn(IV), Mn(III), Ni(III), and Co(II) ions, respectively. All calculations are performed using the VASP code, where we employed a Gamma-centered Monkhorst-pack grid of size 8 x 8 x 8 and a cut off energy of 400 eV for the plane-wave basis.

First, we used HSE06+D3 with an exact exchange mixing parameter (α) of 0.22 to be consistent with Peng et. al.'s work [1]. We have summarized the calculated U value for these ions in Table S1 below.

	HSE06($\alpha = 0.22$)+D3 MM (μ_B)	r ² SCAN+rVV10+U MM (μ_B)	U (eV)
MnO ₂	3.023	3.023	1.41
KMnO ₂	3.933	3.933	1.26
KNiO ₂	1.098	1.098	1.53
CaCoO ₂	2.663	2.663	0.55

TABLE S1. The U value determined by equating the magnetic moments (MM) of HSE06+D3 ($\alpha = 0.22$) and r²SCAN+rVV10+U, using the HSE06+D3 ($\alpha = 0.22$) geometry for both functionals.

We could not use this method to determine the U values for Ni(IV) and Co(III) ions using NiO₂ and KCoO₂ systems because the MM of Ni(IV) and Co(III) ions in NiO₂ and KCoO₂ is zero, largely independent of the U value, in the r²SCAN+rVV10+U calculation. So, we used the same U values for Ni(IV) and Co(III) as determined for Ni(III) and Co⁺⁴, respectively. We used the U values determined in Table S1, as well as U values from the literature [2], and calculated lattice parameters for MnO₂, NiO₂, and CaCoO₂ unit cells to see how r²SCAN+rVV10+U performs compared to HSE06+D3 with $\alpha=0.22$. The results are summarized in Table S2 below. We see that the lattice constants agree well for r²SCAN+rVV10 and r²SCAN+rVV10+U, but they disagree with HSE06+D3 ($\alpha=0.22$) lattice parameters, especially the c parameter. Probably this is because the D3 parameters were determined for HSE06 at $\alpha = 0.25$, not 0.22. This motivated us to go back to full HSE06.

As above, we again determined U values by comparing the MM of r²SCAN+rVV10+U with the full HSE06+D3 ($\alpha=0.25$) functional. Table S3 below summarizes the result. The U values determined in the Table S3 are closer to the values in the literature, where optimal values for Mn, Ni, and Co ions for r²SCAN are 1.8 eV, 2.1 eV, and 1.8 eV, respectively [2]. The difference in oxidation states of ions could be the cause of the discrepancy. We used the above U values for the r²SCAN+rVV10+U functional and again compared the lattice parameters. The results are summarized in Table S4 below.

System	Method	Lattice Parameters (\AA)			Lattice Angles (Degree)		
		a	b	c	α	β	γ
MnO ₂	r ² SCAN+rVV10	2.82	2.82	9.23	90	90	120
	r ² SCAN+rVV10+U(1.41 eV)	2.83	2.83	9.22	90	90	120
	HSE06($\alpha = 0.22$)+D3	2.83	2.83	9.59	90	90	120
NiO ₂	r ² SCAN+rVV10	2.74	2.74	8.98	90	90	120
	r ² SCAN+rVV10+U(1.53 eV)	2.73	2.73	9.00	90	90	120
	HSE06($\alpha = 0.22$)+D3	2.72	2.72	9.25	90	90	120
KCoO ₂	r ² SCAN+rVV10	2.89	2.89	11.64	90	90	120
	r ² SCAN+rVV10+U(0.55 eV)	2.89	2.89	11.65	90	90	120
	HSE06($\alpha = 0.22$)+D3	2.86	2.86	11.21	90	90	120

TABLE S2. Lattice parameters and lattice angles comparison for r²SCAN+rVV10, r²SCAN+rVV10+U and HSE06($\alpha = 0.22$)+D3 methods for the systems MnO₂, NiO₂ and KCoO₂.

	HSE06($\alpha = 0.25$)+D3 MM (μ_B)	r ² SCAN+rVV10+U MM (μ_B)	U (eV)
MnO ₂	3.036	3.036	1.71
KMnO ₂	3.947	3.947	1.58
KNiO ₂	1.163	1.163	2.06
CaCoO ₂	2.683	2.683	0.91

TABLE S3. The U value determined by equating the magnetic moments (MM) of HSE06+D3 ($\alpha = 0.25$) and r²SCAN+rVV10+U, using the HSE06+D3 ($\alpha = 0.25$) geometry for both functionals.

System	Method	Lattice Parameters (\AA)			Lattice Angles (Degree)		
		a	b	c	α	β	γ
MnO ₂	r ² SCAN+rVV10	2.82	2.82	9.23	90	90	120
	r ² SCAN+rVV10+U(1.71 eV)	2.84	2.84	9.11	90	90	120
	HSE06($\alpha = 0.25$)+D3	2.82	2.82	9.25	90	90	120
NiO ₂	r ² SCAN+rVV10	2.74	2.74	8.98	90	90	120
	r ² SCAN+rVV10+U(2.06 eV)	2.73	2.73	8.98	90	90	120
	HSE06($\alpha = 0.25$)+D3	2.73	2.73	9.03	90	90	120
KCoO ₂	r ² SCAN+rVV10	2.89	2.89	11.64	90	90	120
	r ² SCAN+rVV10+U(0.91 eV)	2.89	2.89	11.65	90	90	120
	HSE06($\alpha = 0.25$)+D3	2.87	2.87	11.61	90	90	120

TABLE S4. Lattice parameters and lattice angles comparison for r²SCAN+rVV10, r²SCAN+rVV10+U and HSE06($\alpha = 0.25$)+D3 methods for the systems MnO₂, NiO₂ and KCoO₂.

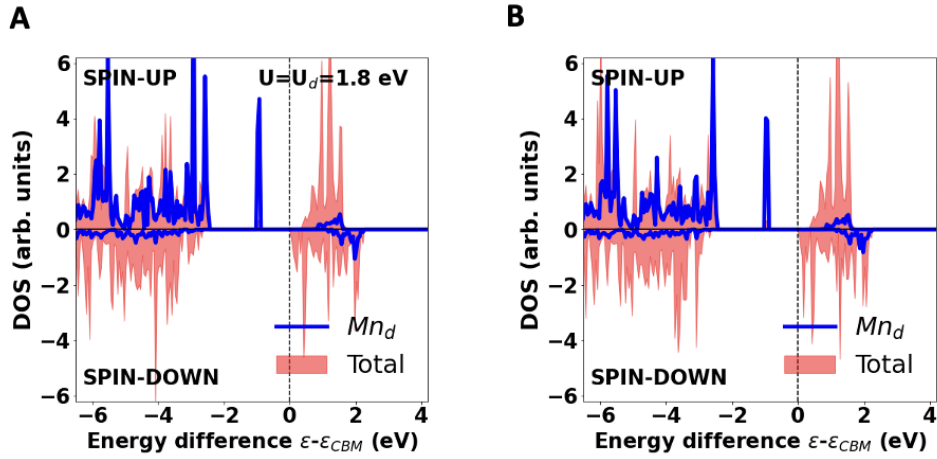


FIG. S1. Spin-resolved density of states per atom using $r^2\text{SCAN}+r\text{VV10}+U+U_d$ (with $U=U_d=1.8$ eV) geometry in a single K-intercalated MnO_2 using (A) HSE06 (with $\alpha=0.22$) and (B) HSE06 (with $\alpha=0.22$)+D3.

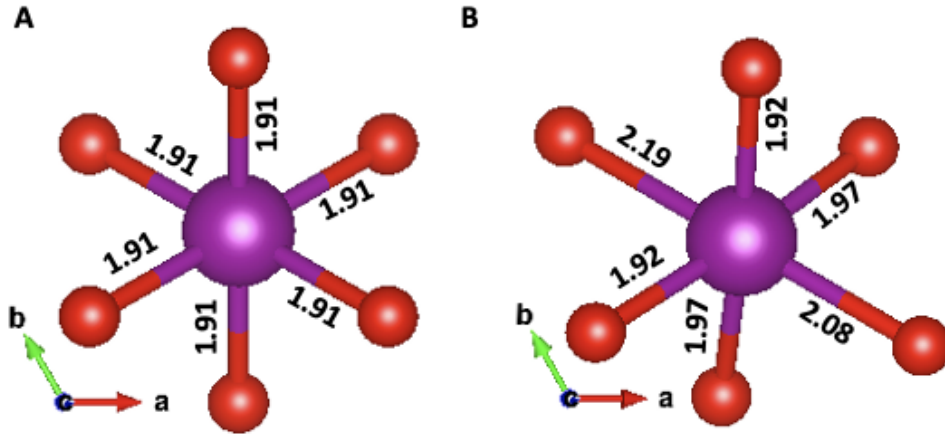


FIG. S2. (A) Mn(IV) - O bond lengths in pristine MnO_2 and (B) defect Mn(III) - O bond lengths in a K-intercalated MnO_2 ($\text{K}_{0.03}\text{MnO}_2$) calculated using the $r^2\text{SCAN}+r\text{VV10}+U+U_d$ (with $U=U_d=1.8$ eV) functional, showing the Jahn-Teller symmetry breaking of the MnO_6 octahedron. All lengths are in angstrom units. The red balls represent O ions and purple Mn ions. In the pristine materials, the three t_{2g} (d_{xy}, d_{yz}, d_{zx}) space orbitals are equally populated, and the two e_g ($d_{x^2-y^2}, d_{z^2}$) spatial orbitals (whose lobes point from the metal cation to the 6 oxygens on the corners of the octahedron) are empty.

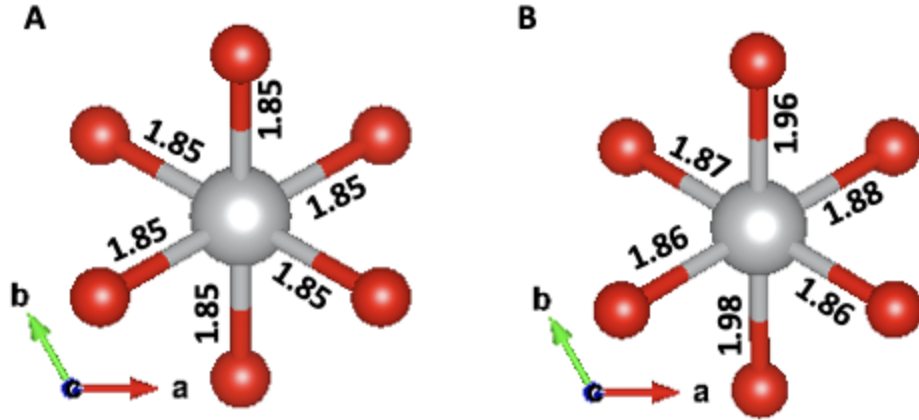


FIG. S3. (A) Ni(IV) - O bond lengths in pristine NiO₂ and (B) defect Ni(III) - O bond lengths in a K-intercalated MnO₂ (K_{0.03}NiO₂) calculated using the r²SCAN+rVV10+U+U_d (with U=U_d=2.1 eV) functional, showing the Jahn-Teller symmetry breaking of the NiO₆ octahedron. All lengths are in angstrom units. The red balls represent O ions and silver Ni ions. In the pristine materials, the three t_{2g} (d_{xy}, d_{yz}, d_{zx}) space orbitals are equally populated, and the two e_g (d_{x²-y²}, d_{z²}) spatial orbitals (whose lobes point from the metal cation to the 6 oxygens on the corners of the octahedron) are empty.}

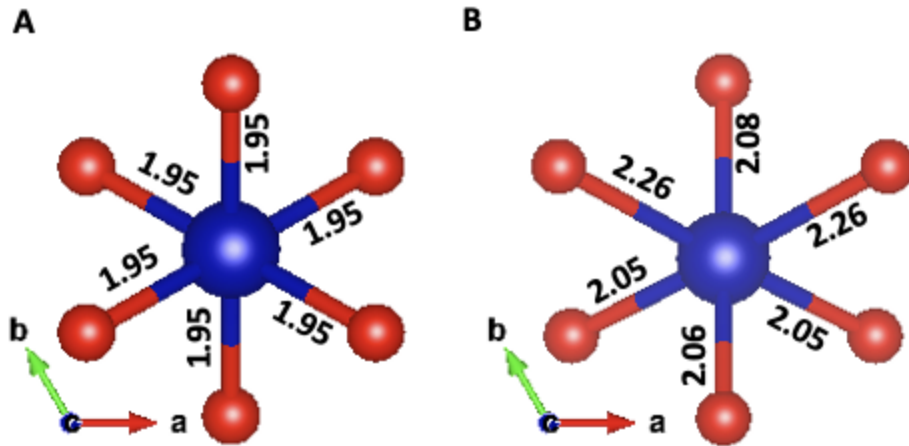


FIG. S4. (A) Co(III) - O bond lengths in pristine KCoO₂ and (B) defect Co(II) - O bond lengths in a K-intercalated KCoO₂ (K_{1.03}CoO₂) calculated using the r²SCAN+rVV10+U+U_d (with U=U_d=1.8 eV) functional, showing the Jahn-Teller symmetry breaking of the CoO₆ octahedron. All lengths are in angstrom units. The red balls represent O ions and blue Co ions. In the pristine materials, the three t_{2g} (d_{xy}, d_{yz}, d_{zx}) space orbitals are equally populated, and the two e_g (d_{x²-y²}, d_{z²}) spatial orbitals (whose lobes point from the metal cation to the 6 oxygens on the corners of the octahedron) are empty.}

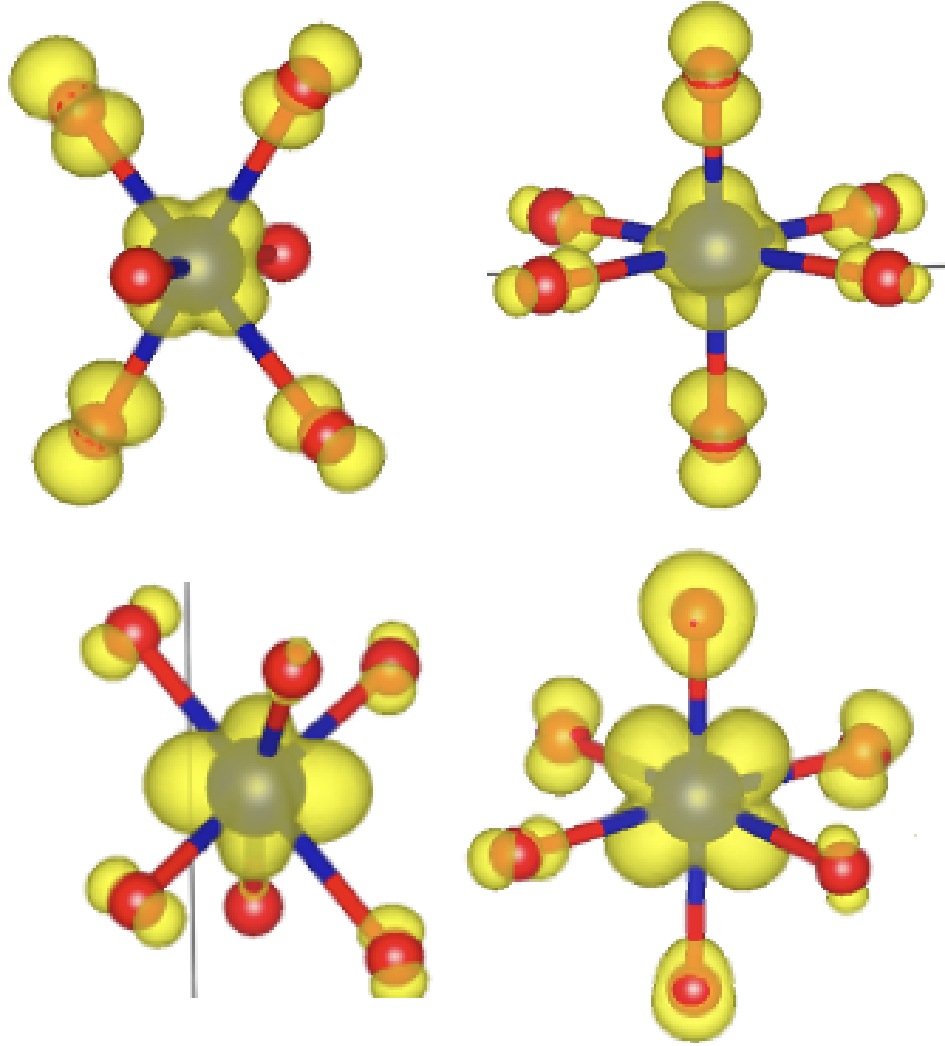


FIG. S5. $r^2\text{SCAN} + r\text{VV10} + U + U_d$ ($U = U_d = 1.8$ eV) based total charge density plots of four localized orbitals in the band gap region of $\text{K}_{1.03}\text{CoO}_2$ around the defect Co(II) ion. The plots in the upper panel correspond to the two highest occupied orbitals in the spin up channel and clearly show them to be the e_g orbitals. The lower panel corresponds to the two highest occupied orbitals in the spin down channel and shows them to be the t_{2g} orbitals.